HHS Public Access

Author manuscript

Exp Cell Res. Author manuscript; available in PMC 2015 June 25.

Published in final edited form as:

Exp Cell Res. 2014 January 1; 320(1): 79–91. doi:10.1016/j.yexcr.2013.09.016.

Galvanic microparticles increase migration of human dermal fibroblasts in a wound-healing model via reactive oxygen species pathway

Nina Tandon[a,b,1], **Elisa Cimetta**[a,1], **Aranzazu Villasante**[a], **Nicolette Kupferstein**[b], **Michael D. Southall**[c], **Ali Fassih**[c], **Junxia Xie**[c], **Ying Sun**[c], and **Gordana Vunjak-Novakovic**[a,*]

Nina Tandon: nmt2104@columbia.edu; Elisa Cimetta: ec2438@columbia.edu; Aranzazu Villasante: av2499@columbia.edu; Nicolette Kupferstein: sinens@cooper.edu; Michael D. Southall: msoutha@its.jnj.com; Ali Fassih: afassih@its.jnj.com; Junxia Xie: junxiaxie@yahoo.com; Ying Sun: Ysun@its.jnj.com; Gordana Vunjak-Novakovic: gv2131@columbia.edu

[a]Columbia University, Department of Biomedical Engineering, 622 West 168th Street, MC 104B, New York 10027, NY, USA

[b]The Cooper Union for the Advancement of Science and Art, Department of Electrical Engineering, 41 Cooper Square, New York 10003, NY, USA

[c]Johnson and Johnson Skin Research Center, Johnson & Johnson Consumer and Personal Products Worldwide, Division of Johnson & Johnson Consumer Companies, Inc., Skillman 08558, NJ, USA

Abstract

Electrical signals have been implied in many biological mechanisms, including wound healing, which has been associated with transient electrical currents not present in intact skin. One method to generate electrical signals similar to those naturally occurring in wounds is by supplementation of galvanic particles dispersed in a cream or gel. We constructed a three-layered model of skin consisting of human dermal fibroblasts in hydrogel (mimic of dermis), a hydrogel barrier layer (mimic of epidermis) and galvanic microparticles in hydrogel (mimic of a cream containing galvanic particles applied to skin). Using this model, we investigated the effects of the properties and amounts of Cu/Zn galvanic particles on adult human dermal fibroblasts in terms of the speed of wound closing and gene expression. The collected data suggest that the effects on wound closing are due to the ROS-mediated enhancement of fibroblast migration, which is in turn mediated by the BMP/SMAD signaling pathway. These results imply that topical low-grade electric currents via microparticles could enhance wound healing.

*Corresponding author: Fax: +1 212 305 4692.

[1]These authors contributed equally to this work.

Ethics statement

All studies have been conducted in accordance to approved protocols at the Columbia University, and the ethical and responsible conduct of research.

Conflict of interest

The work was funded in part by Johnson & Johnson, Contract CU10-0162 to GVN.

Keywords

Galvanic particles; Reactive oxygen species; Fibroblasts; Wound healing

Introduction

Electrical signals regulate the behavior of excitable cells including those found in skin, heart, skeletal muscle, neural and vascular tissue. These signals are essential to a range of biological processes, including vision, hearing, heartbeat, and digestion [1]. Furthermore, transient bioelectrical signals have been implicated in cell proliferation, migration and differentiation during embryogenesis, wound healing, and tissue regeneration [2].

Electric fields were detected within endogenous wounds more than 150 years ago [3]. During wound healing, outward electrical currents of 10–100 μA/cm^2 create a voltage drop of ~600 mV/cm within the first 125 μm of the extracellular space [4]. These fields are due to a short-circuiting of the transepithelial potential gradient, which arises due to separation of ionic charges across the intact epithelium. When the skin is cut, a large steady electric field arises immediately and persists for hours at the wound edge, as currents pour out from underneath the wounded epithelium [5].

Many types of cells [6,7], including some skin cell types (e.g., fibroblasts [8–10] and keratinocytes [11,12] but not melanocytes [13]), exhibit directional migration (i.e., galvanotaxis) when exposed to direct currents of physiologically relevant magnitudes. These effects have implicated that wound-generated electric fields provide migrational cues that contribute to wound healing (see [14] for a review), and motivated the application of exogenous electric fields to enhance the healing of chronic wounds, in clinical practice for many decades [15,16].

Some of the new treatment modalities currently under research include topical application of galvanic particles dispersed in cream or gel. In one application, zinc micro-particles were deposited with copper specks and used to deliver low-level electrical stimulation to intact skin and primary keratinocytes [17]. Topical application on intact skin was shown to generate an electric potential of 1.5 V/cm, and application to primary keratinocytes in culture enhanced the production of reactive oxygen species (ROS), and inhibited secretion of inflammatory cytokines. These results are quite interesting when considering that after the initial phase of wound healing, inflammation is reduced, and cellular interactions are dominated by the interplay of keratinocytes and fibroblasts [18]. In fact, during skin wound healing, keratinocytes, which make up the predominant cell type in the epidermis, stimulate fibroblasts to synthesize growth factors, which in turn stimulates keratinocyte proliferation in a double paracrine manner [19].

Starting from this evidence, we were interested in exploring the mechanism of action of galvanic microparticles on human dermal fibroblasts. We sought the putative mediator between the microparticles and the cells, which could trigger responses promoting/hindering wound healing. For example, it is known that reactive oxygen species (ROS) are potent effectors in directing cell fate. It is likely that the galvanic microparticles could

generate microcurrents capable of inducing or mimicking ROS production. We thus hypothesized that these microcurrents will enhance the migration of dermal fibroblasts, and thereby accelerate wound healing, via increased production of ROS. To test this hypothesis, we treated adult dermal fibroblasts with low concentrations of zinc–copper galvanic microparticles, in a model system designed to mimic the skin dermis, epidermis, and the topical cream. We observed a ROS-mediated increase in fibroblast migration, and determined that this increase was induced by a BMP/Smad signaling pathway.

Methods

Characterization of galvanic microparticles

Surface potentials of 8 μm diameter zinc–copper microparticles (provided by Johnson and Johnson Consumer Companies, Inc., Skillman, NJ) were mapped using a Park Systems Electron Force Microscope XE-70 in non-contact mode performing both scanning Kelvin probe microscopy (SKPM) and electric force microscopy (EFM). Topography and potential scans were obtained of grounded, mechanically steady particles, de-noised, and peak-to-valley potentials (Rpv) were then measured as the difference between maximum and minimum measured potentials on the surface. The average size of the zinc (Zn) particles, the copper (Cu) deposits coated onto the Zn, and average distance between Cu deposits were calculated from pixel values of scanning electron microscopy (SEM) images taken using a JEOL 6400-F system at 35,000 × magnification. 90 measurements were averaged to determine Cu deposit size, and 30 measurements were averaged for distance measurements (Fig. 1). In order to perform mathematical modeling, a custom MATLAB script was used to calculate the number of Cu deposits per Zn sphere and the fraction of surface coated by Cu deposits from the measured Cu deposit size and distance measurements, making the approximation that Cu deposits were uniformly distributed. Using the known weight of Cu, the volume per Cu speck and Cu deposit height were calculated by approximating each deposit as a semi-spherical cap and calculating the amount that the sphere required to be recessed.

Modeling of the electrical field

Finite element numerical simulation was performed to predict the electrical field distribution around the microparticles using commercially available software (Multiphysics, Comsol, electrostatics module). The electroquasistatic approximation is considered appropriate for simple cases such as homogeneous, isotropic media, where the system under consideration is much smaller than the wavelengths of interest [20,21]. For this study, an isotropic medium with conductance of 1.5 S/m (a value reported previously for cell culture medium, [22]) was assumed and the electric fields were calculated by solving Maxwell's equations with the quasistatic approximation [21].

To model the geometry of the microparticle in two dimensions, the average diameter of Cu deposits, calculated arc length distance from SEM images (see “characterization of galvanic microparticles” section), and the measured potential difference from SPKM scans were used. The protrusion of the Cu deposits was assumed to be negligible based on calculations of deposit height made from known mass ratio of Zn to Cu (Fig. 1). In addition, the well

plate surface was assumed to provide an electrically insulating boundary condition, and equations were solved using the software's finest possible triangular mesh element settings (ranging from 3.7–1.4 $\times 10^4$ μm^2, corresponding to an average element size of 91 μm^2).

Cell preparation

Primary human dermal fibroblasts from a 35-year old female donor (ATCC), between passages 5 and 9, were used in all experiments. Stock cultures were maintained in monolayers grown in plastic cell culture dishes from Falcon Labware (BD Biosciences, San Jose, CA) using fibroblast cell culture medium (Dulbecco's high glucose modified Eagle's medium (DMEM 11965 basal medium), 1% 100 mM sodium pyruvate, 1% penicillin (10,000 U/ml)/streptomycin (10,000 μg/ml), and 10% fetal bovine serum (all from Gibco, Grand Island, NY). The cultures were passaged at 80% confluence, and incubated at 37 °C in a humidified atmosphere of 5% CO_2.

In vitro model system of skin with galvanic microparticles

The model system for studying the effects of galvanic microparticles on cultured dermal fibroblasts was designed to mimic topical application of microparticles suspended in gel onto the epidermis with underlying dermal layer (Fig. 2A, left-hand side). A three-layered model of skin consisting of human dermal fibroblasts was constructed in hydrogel (mimic of dermis), a hydrogel barrier layer (mimic of epidermis) and galvanic particles in hydrogel (mimic of a cream containing galvanic particles applied to skin) (Fig. 2A, right-hand side).

First, cells were placed on the bottom surface of 24-well tissue culture plates (BD Biosciences), and allowed to attach for 24 h. Cells were plated at 70,000 cells per well for cellular viability, ROS, and wound healing studies, and at 30,000 cells per well for RNA quantification studies. Next, a 200 μm thick layer of hydrogel (40 μL volume, 50% cell culture media/ 50% growth-factor reduced Matrigel from BD Biosciences) was applied on top of the cell layer, to simulate the horny barrier layer of the epidermis. After near-complete gelation of this layer (3 min incubation at 37 °C), a second hydrogel layer, 750 μm high and 150 μL in volume containing suspended microparticles was applied, to simulate topical application of galvanic microparticles. After gelation of this second layer, 300 μL of cell culture media was added to each well. In order to prevent gelation before application of the barrier and microparticle layers, the 50% cell culture medium/50% Matrigel hydrogels were maintained on ice before application to cells. All galvanic microparticle suspensions were prepared fresh for each experiment.

Cellular viability and survival

Cellular viability and survival were assessed for human adult dermal fibroblasts after 24 h of treatment with galvanic microparticles. Cellular viability was assessed via LIVE/DEAD® Viability/ Cytotoxicity Assay Kit using the combination of Calcein AM and Ethidium homodimer-1 (Invitrogen) following the manufacturer's instructions. Fluorescent images (495 and 488 nm, for green and red live and dead stains, respectively) were taken after 30 min incubation with reagents at 37 °C, 5% CO_2. Fluorescence images were merged with green (live) and red (dead) channels; no postprocessing/enhancing was performed. Cell survival was assessed via image analysis of cells stained with the fluorescent 4,6-

diamidino-2-phenylindole (DAPI) nuclear stain (Vecta Shield) using a custom MATLAB function based on previous methods [23] that identify and count cell nuclei. Cell counts were normalized versus t_0 control (cells immediately prior to treatment). All images were taken with fluorescent microscope at 10 × magnification (Olympus IX81, Hamamatsu C4742-95 high resolution camera).

Generation of reactive oxygen species

Cellular expression of ROS was assessed for human adult dermal fibroblasts after 3 h of treatment with galvanic microparticles. Prior to treatment, cells were rinsed once with phosphate-buffered saline solution (PBS) for 2 min (Corning Cellgro) before incubation for 40 min at 37°C, 5% CO_2 in PBS containing 100 μm of the general oxidative stress indicator CM-H2DCFDA (Invitrogen), which is one of the most widely used techniques for directly measuring the redox state of a cell, is extremely sensitive to changes in the redox state of a cell, and can be used to follow changes in ROS over time [24]. After incubation in the dye, cells were then rinsed in PBS again for 2 min before treatment with galvanic microparticles (suspended in PBS) at varying concentrations (wt/vol). Fluorescence measurements were taken at the time of galvanic microparticle application (t = 0), and then 5, 10, 15, 30, and 60 min, 2 h, and 3 h later. Measurements were taken with excitation and emission wavelengths of 485 and 530 nm, respectively, a gain of 200, and with 9 measurements taken at the center of each well (border of 4 mm) (Tecan Infinite® 200 PRO). The measured values were normalized to the corresponding values at time zero. To validate the ROS acquisition methodology, green fluorescent images (excitation ~495 nm, emission ~515 nm) were taken at t = 0, 5 min, 30 min and 3 h at 10 × magnification (Olympus IX81, Hamamatsu C4742-95 high resolution camera).

Wound-healing assay

Single vertical scratches were made through the centers of monolayers of human adult dermal fibroblasts using a 10 μL pipette tip. Cell culture media was then gently aspirated, and a 40 μL layer of 50% Matrigel/50% cell culture media was then applied to the cells. After gelation, an additional 150 μL layer of galvanic microparticles suspended in 50% Matrigel/50% cell culture media was applied and allowed to gel. 300 μL of cell culture media was then added to each well.

Images were taken in each well under bright field microscopy at 10 × magnification (Olympus IX81, Hamamatsu C4742-95 high resolution camera) at the time of galvanic microparticle application (t = 0), after 1, 2, and 3 h, and processed according to our established protocols, using custom MATLAB software [25]. Briefly, an edge detection algorithm using a Sobel filter was used to identify the edge of the scratch based on where the gradient of the intensity of the image was greatest. Once the edges of the scratch were determined, the areas containing cells were defined to be white and the area of the scratch was defined to be black. Then, for every row of pixels, the number of black pixels existing between white ones was found. The image was then segmented into 5 equal sections, and the average pixel length for each section was found. The decrease in the width of the scratch was used to calculate the rate of migration of the cells into the wound area.

RNA quantification

qPCR primer sequences were retrieved from the online Primer-Bank (http://pga.mgh.harvard.edu/primerbank) (bank primer IDs GAPDH: 83641890b1, BMP6: 133930782b1, ID1: 341865545c1, SMAD7: 299890804c2, respectively) and custom primers based on these sequences were synthesized (Invitrogen). Total RNA was obtained using Trizol (Life Technologies) following the manufac turer's instructions. Total RNA (2 μg) preparations were treated with pre-formulated, pre-packaged “Ready-To-Go You-Prime First-Strand Beads” (GE Healthcare) to generate cDNA according to the manufacturer's protocol. Quantitative real-time PCR was performed using Fast SYBR Green Master mix (Invitrogen). Quantifications were made applying the ΔCt method.

Statistical analysis

Results are presented as average±standard deviation. Differences between groups were analyzed by single-tailed students *T* test for experiments with sample number $n=5$ (using Microsoft® Excel software), and by Wilcoxon Rank Sum Test (http://www.socr.ucla.edu/) for experiments with sample numbers $n<5$. In all cases, $p\leq 0.05$ was considered significant.

Results and discussion

Characterization of Zn–Cu galvanic microparticles

Galvanic Zn–Cu microparticles were designed based on the concept of a galvanic electrochemical cell. In an electrochemical cell, two metals of different electrochemical properties, such as Zn and Cu, are placed in baths of their respective salts with a salt bridge or a porous material connecting them. Due to their electrode potential differences, Zn undergoes oxidation and loses electrons, becoming the anode of the cell, while Cu is reduced receiving the free electrons, becoming the cathode of the cell. For standard zinc and cooper materials, the electric potential produced is approximately 1.1 V [26,27].

For this study, galvanic zinc–copper microparticles were produced by reacting aqueous Cu ions onto a pure Zn particle surface through a displacement oxidation–reduction reaction, resulting in a Zn surface covered with smaller Cu deposits. As with any combination of dissimilar metals placed in an electrolyte solution, such as cell culture media [22], the less noble (base) metal will experience galvanic corrosion [27]. In the case of the microparticles used in this study, the Zn surface acts as an anode and the Cu deposits act as a cathode, thus producing an electric field [17]. In this study, several forms of Zn–Cu mircoparticles were produced, with increasing Cu mass percentages (as compared to the Zn).

From scanning electron microscopy (SEM) topography scans, Cu deposits are apparent on the particles on which Cu was deposited onto Zn microparticles (Fig. 1A), although not on the Zn particles. Spot analysis of the microparticles, performed via Time-of-Flight Secondary Ion Mass Spectrometry (TOF-SIMS) and Energy Dispersive Spectroscopy, confirmed that the deposits were Cu, and analysis of raw particles confirmed the absence of Cu (data not shown). From scanning Kelvin probe microscopy (SKPM) images (Fig. 1B), peak-to-valley potentials (Rpv) were observed to increase with Cu mass percentages, from 353 mV for 0.1% Cu on Zn, to 770 mV for 0.75% Cu on Zn, respectively (Fig. 1C).

Worth noting is that although peak-to-valley potentials were observed to increase with increasing the Cu/Zn ratio, the measured potentials did not approach the values expected for the galvanic series of these dissimilar metals (i.e., 1.1 V, [26]). This is likely due to the presence of certain non-idealities characteristic of highly non-linear electrochemical systems such as the ones described here (e.g., ionic composition, resistance to corrosion, geometry, surface area, roughness, etc.) [28]. Therefore, for the purposes of modeling the electric fields produced by the particles in the experimental system, the respective peak-to-valley potentials for 0.1% and 0.75% Cu on Zn were used, along with other parameters calculated from SEM and SKPM data (Fig. 1D). It would be interesting in future work to see how close a system of microparticles with increasing amounts of Cu on Zn might approach the predicted potential.

The model system used in this study for culturing human dermal fibroblasts with Zn–Cu galvanic microparticles (Fig. 2A) consists of a 200 μm barrier layer of Matrigel on top of a monolayer of cells which is meant to simulate the epidermal horny layer of skin, and superficial layer of Matrigel containing a suspension of microparticles that simulates the topical application of crème containing microparticles to the epidermis. In order to model the voltage field around the applied microparticles, a single microparticle's placement of copper deposits was first modeled in three dimensions (3D) (Fig. 2B) to determine whether a 2-dimensional (2D) approximation could be made. Given the high density of the Cu deposits (~17,000 deposits/microparticle), the generated voltage field was considered to be radially symmetric as to allow the model system to be approximated by using a 2D cross section (fitting a total of 232 Cu deposits per microparticle).

Inspection of the color-map showing electric potential surrounding an individual microparticle (Fig. 2C) indicates that although a fairly strong electric field is induced by the potential difference between Zn and Cu, this field fails to propagate beyond ~100 nm away from the microparticle's surface, and so this electric field is unlikely to produce a non-negligible effect on the cells cultured in the model system under study. Despite the shallowness of this electric field, however, given that the dominant anion in the cell culture medium is chloride, a strong electrochemical corroder of zinc, the Cu–Zn microparticles produce stray electrons close to the microparticles, which may in turn trigger cellular responses [29]. Using the currents measured in previous studies of Zn–Cu microparticles in PBS [17], the currents generated by the microparticles at the concentrations used in this study were calculated to be 80 and 175 μA/mg for 0.1% and 0.75% Cu on Zn, respectively (Fig. 2D). Interestingly, the current densities of ~0.03–6 $\mu A/cm^2$ for a 24-well culture plate are similar to those measured for wounded skin cells (4 $\mu A/cm^2$) [30]. Correlating this range of working concentrations and strengths of galvanic microparticles to the cellular viability and wound-healing is therefore of particular interest.

Cells maintain viability in the presence of galvanic microparticles

Using live/dead staining, it was found that at low concentrations of applied galvanic microparticles cells appeared elongated, with nearly 100% of cells staining as live. This elongation is consistent with the healthy fibroblastic phenotype [31]. At higher concentrations, however, cells began to show signs of deterioration appearing more rounded,

with interspersed non-viable cells. This effect was even more pronounced with the higher copper concentration microparticles (Fig. 3A).

Using DAPI nuclear staining, it was observed that although the application of higher concentrations of galvanic microparticles appeared to reduce cell proliferation as compared to control after 24 h, low concentration of higher activity microparticles (0.75% copper) showed a trend of enhancing cell proliferation (although not to a statistically significant extent) (Fig. 3B). Applying the simple exponential doubling time formula $N = N_0 2^{24/d}$ where N corresponds to the number of cells 1 day after seeding, N_0 corresponds to the initial number of seeded cells, and d corresponds to the doubling period, in hours, we may calculate that these cells (i.e., 0.75% Cu on Zn at concentration of 0.0005%) doubled every 15.6 h.

It is of note that measurement errors may be introduced with this method, as several rinsing steps are involved, and the cells may be detached from the culture substrate in a non-uniform manner. In addition, this method may confound effects due to proliferation and attachment strength. Fibroblasts exhibiting an inflammatory phenotype are known to display reduced tension and proliferation [31], and reduced adhesion strength while migrating in the presence of electric fields [32]. Although there is no sufficient statistical power to unequivocally conclude significant treatment effects, data suggest that application of galvanic microparticles in the 0.0005–0.005% range is safe to dermal fibroblast cells. This range was thus used in all subsequent studies.

Galvanic microparticles alter migration of human dermal fibroblasts

The presence of galvanic microparticles within a wound-healing model *in vitro* (0.75% copper, 0.001% concentration) increased the speed of wound closing as compared to control (Fig. 4A). Other preparations of galvanic microparticles also tended to accelerate wound closing (e.g., 0.1% Cu on Zn at 0.005% concentration; 0.75% Cu on Zn at 0.0005% concentration), but without statistical significance (Fig. 4B). Given that the experimental time points for the wound healing assay are significantly lower than the fastest doubling time for the cells (i.e., 15.6 h for 0.75% Cu on Zn at concentration of 0.0005%), we believe the predominant mechanism of wound closure to be cell migration as opposed to cell division. From this perspective, it is interesting to note that the measured speeds of wound closing in the fastest group and the controls were similar to the corresponding values found in studies of fibroblasts migrating in response to spatially uniform electric fields (20–30 μm/h in physiologic electric fields, ~10 μm/h for unstimulated controls) [25,32].

However, in contrast to cells exhibiting directed migration in response to the presence of an electric field, in this study, it is unlikely that the electric field produced from the galvanic microparticles is providing a directional galvanotactic cue to the migrating fibroblasts. Although the current densities calculated for microparticles applied in our model system were similar to those measured for wounded skin [30], finite element modeling showed that the electric field dissipated within nanometers of the edges of the microparticles (Fig. 2C), far shorter than the ≥200 μm distance between the microparticles and the cell monolayer (Fig. 2A). Instead, it is more likely that the currents generated by the microparticles,

although similar to current densities in wounded skin cells, would be acting indirectly to stimulate the migration of the cells.

In vivo, the epithelial wound site normally represents a cathode with induced wound lateral currents [33]. Epithelial cells and fibroblasts align parallel to the wound edge and perpendicular to the wound vector; epithelial cells also show alignment of cleavage planes of cell division with the wound axis [34,35]. The effects of physiological electric fields on the direction of migration of human dermal fibroblasts are not well understood: studies have shown that the application of physiological electric fields may have differing effects on migration of human dermal fibroblasts than non-dermal fibroblasts and keratinocytes, in terms of both timing and directionality [8,9,11]. Taken together, these observations have led us to investigate whether a soluble mediator could instead be the trigger to the observed cellular responses upon exposure to the microparticles. From this perspective, reactive oxygen species (ROS), which have been associated with applied electrical fields in cultured cells [36–38], are present during dermal wound healing (reviewed in [39]), and have been shown to act within cells to promote proliferation, migration and adhesion of cells (reviewed in [40]), are of particular interest. In addition, past studies showed that galvanic microparticles similar to those used in this study might enhance ROS production in human keratinocytes [17]. We therefore measured the ROS production in response to galvanic microparticles in the experimental group exhibiting the fastest wound healing (Fig. 5).

Generation of ROS by galvanic microparticles

Human dermal fibroblasts subjected to galvanic microparticles and hydrogen peroxide (H_2O_2) showed increases in fluorescence with continued exposure (Fig. 5A), indicating comparable increases in ROS production (Fig. 5B). The fluorescent dye used in this study has been traditionally been used to detect ROS, and shown to be highly photosensitive and susceptible to light-induced auto-oxidation, resulting in background fluorescence [41], which may in part explain the increase in fluorescence of the non-stimulated control samples. In spite of the measurement variability, these results are consistent with studies in which electrical fields were associated with oxidative stress in cultured cells [36–38]. These results are also consistent with increases in ROS observed in primary skin keratinocytes cultured with galvanic microparticles similar to those used in our study [42]. Interestingly, in that study, galvanic microparticles also exhibited increases in ROS and the reduction in inflammatory cytokines, neither of which were observed with the application of either Cu (itself a free radical [43]), or Zn (a redox-inactive metal [44]) alone, suggesting that the combination of these elements, whether in the microparticle configuration or otherwise, was responsible for the observed effects. Finally, the reduction in pro-inflammatory cytokine interleukin-1 alpha (IL-1α) that was observed with the application of the galvanic microparticles was reversed with the application of the Catalase enzyme, which catalyzes the decomposition of H_2O_2, suggesting that the presence of ROS was also involved in the anti-inflammatory effect.

When considering the evidence that ROS might be involved in the observed increased speed of migration in this study, it is worth noting that the galvanic microparticles were added ≥200 μm away from the fibroblasts within our model system. ROS, by their very nature,

however, are quite short-lived, reacting quite quickly near the site where they are formed, with diffusion distances ranging from ~3 nm for the hydroxyl radical to 100 μm for peroxynitrate (although reactions with bicarbonate and thiols in the cell/culture media may decrease the diffusion distance to ~9 μm) [45]. Nonetheless, when free radicals steal an electron from a surrounding compound or molecule a new free radical is formed in its place, which in turn looks to return to its ground state by stealing electrons from nearby cellular structures or molecules. Thus ROS may originate chains of reactions much further from site of initial production (i.e., 'radicals beget radicals') [46]. For this reason, we propose that it is therefore possible to view galvanic microparticles as local sources of "controlled-release" ROS, in contrast to temporally-discrete application of oxidants such as H_2O_2. From this perspective, the ROS concentration is clearly important, given that high concentrations of free radicals have been shown to cause detachment and rounding of fibroblasts, whereas lower concentrations (e.g., 1 μM H_2O_2) have been shown to increase their density [47].

Our results are also consistent with recent studies showing that ROS may act beneficially as signaling molecules regulating various cellular functions, including proliferation, migration and adhesion of cells (reviewed in [40]). The general mechanism by which ROS are thought to signal proliferation, migration and adhesion of cells is as follows: (i) in response to stimuli, such as tissue wounding, or growth factors, ROS are generated at the surface of cells or within intracellular compartments, such as endosomes, by nicotinamide adenine dinucleotide phosphate (NADPH) oxidases [48–50]; (ii) once inside the cell, the ROS react with specific proteins to modulate protein function, driving cellular processes such as migration. Notable examples include promotion of vascular endothelial growth factor VEGF signaling via oxidative inactivation of protein tyrosine phosphatases (PTPs) [51], and covalent crosslinking [52] or tyrosine phosphorylation [52–54] of epidermal growth factor receptor EGFR. The exact mechanism by which activation of cell surface receptors trigger NADPH oxidases to generate ROS during cell migration is not entirely clear; nor are the exact identities of redox-regulated proteins that are oxidized during cell migration or adhesion [40]. Nonetheless, either directly or indirectly, hydrogen peroxide is known to cause selective post-translational modifications of proteins, modulating their function and influencing cell migration [40]. Further studies utilizing redox enzymes (such as catalase), one of the newer, more specific ROS dyes (e.g., genetically encoded redox probes [55]) or inhibition of NADPH oxidase could further elucidate the role of ROS in the observed increase in cellular migration in this study.

Although the understanding of redox control of wound healing is in its nascent stage, there is also evidence in the literature to support the role of ROS in wound healing. It is known, for example, that wounds generate ROS, specifically H_2O_2, in phylogenetically diverse organisms, including plants, *Drosophila melanogaster*, zebrafish, and mammals (listed in [56]), and that many redox-sensitive processes drive dermal tissue repair, at all stages: inflammation, proliferation and maturation [39]. ROS, for example, are known to regulate blood coagulation and thrombosis, chemotaxis, positive and negative control of the inflammatory response, and the expression/function of several growth factors [39].

When relating this evidence to the study presented here, it is worth noting that fibroblasts are most active in the later stages of wound healing: during the proliferation phase,

fibroblasts enter the wound site to replace the provisional matrix established by keratinocytes with granulation tissue composed of fibronectin and collagen [57], and later, as endothelial cells revascularize the damaged area, fibroblasts organize wound contraction [58]. During these processes, fibroblasts secrete and are regulated by a number of molecular signals (reviewed in [59]), many of which are known to be subject to redox/oxidant regulation, including (but not limited to): insulin-like growth factor 1 (IGF-1), fibroblast growth factor (FGF), transforming growth factor-β (TGF-β), nerve growth factor (NGF), bone morphogenic protein-6 (BMP6), and several of the interleukin family of proteins [39,60,61]. Of these, BMP6 is of particular interest, given that fibroblasts are the main producer of BMP-6 during wound healing [62], and that it is observed in the regenerating epidermis at the wound edge as well as in fibroblasts of the granulation tissue [63]. For these reasons, we decided to analyze the response of fibroblast gene expression of BMP6 in response to the application of galvanic microparticles.

Gene expression

Expression of bone morphogenetic protein 6 (BMP6) has been demonstrated in multiple tissues, including bone, brain, lung, kidney, heart, skin and liver [64,65]. In skin, BMP6 signaling has been found to regulate the developing and postnatal skin, control cellular proliferation, differentiation, and tissue remodeling, as well as a variety of pathological processes, including wound healing, psoriasis, and carcinogenesis (reviewed in [66]). Basal expression in adult skin is typically at very low levels, but pathological conditions such as wound healing induce increased expression of BMP6 [67,68] in both keratinocytes and fibroblasts [63,68]. It has been suggested that BMP signaling regulates the wound-healing process in a spatial and temporally-regulated manner [68] by changing the proliferative activity and/or differentiation of epidermal keratinocytes and by altering the collagen-producing activity of dermal fibroblasts [63,66].

In this study, gene expression was analyzed in human dermal fibroblasts in response to 0.75% Cu/Zn galvanic microparticles at the concentration of 0.001%. Significant increases in expression of BMP6, SMAD7 and ID1 mRNA genes were observed (Fig. 6A). The upregulation of BMP6, SMAD7 and ID1 is consistent with what is known about the canonical BMP signaling pathway and skin homeostasis. In the canonical BMP/Smad pathway BMP6 dimers, once secreted, bind simultaneously to complexes consisting of at least one type-I and one type-II receptor (BMPR-I and BMPR-II) [69], inducing phosphorylation of BMPR-I by BMPR-II which, in turn, phosphorylates a subset of Smad proteins (Smad1, Smad5, and Smad8) [64,70] which regulate Smad7 [71] and have negative feedback to BMP6 [66] and Id1 [72].

A proposed role for BMP6 signaling pathway in the study presented here could be either via ID1, stimulating proliferation and stimulation of cell motility after skin injury [73] and inducing ROS production [74], or via SMAD7, which stimulates wound healing [71] (Fig. 6B). Possible mechanisms of BMP6 stimulation by galvanic microparticles could be related to the regulation of phosphorylation of Smad1/5/8 by iron [75] and gene expression of Bmp6, Smad7 and Id1 [76]. In this case, iron, by virtue of its ability to accept or donate electrons, acts as a prooxidant. Although this pathway has not been studied in the skin, it is

interesting to note that iron may be released from hemoglobin after exposure to ultraviolet radiation during oxidative stress [77,78]. It is possible that the galvanic microparticles are mimicking these iron effects in the skin through production of free electrons and BMP/Smad canonical pathway activation.

Given that trace elements Cu and Zn both play critical roles during development and wound healing [79–82], and that the effectiveness of Zn with respect to wound healing may be dependent on the presence of other trace elements (including copper and/or selenium) [83], we cannot rule out other plausible mechanisms of action of the particles involving non-ROS-related pathways. There are a large number of Cu and Zn transporters, for example (in mammals, an array of zinc transporters is encoded by at least 27 genes from 3 families, reviewed in [84], and two mammalian copper transporters play essential roles during development and homeostasis, reviewed in [85]). It is therefore conceivable that Cu and/or Zn may be acting on trace metal transporters in fibroblasts. From this perspective, future studies of the effects of the galvanic microparticles on calcium flux would be particularly interesting, given calcium's association both with ROS-related events and tissue regeneration [56] and recent evidence linking L-type and T-type calcium channel expression to Zn transporter activity [86].

Summary and future work

The presence of galvanic microparticles in a three-layered model of human skin containing human dermal fibroblasts resulted increased fibroblast migration, and increased ROS, correlated with increased expression of the BMP/Smad signaling pathway. Looking ahead to future studies, it would be interesting to further explore the mechanism of action, by exploring whether application of other pro-oxidants alone (e.g., iron, hydrogen peroxide, copper at higher concentrations than in previous studies, etc.) could induce similar effects with respect to gene expression. In addition, more direct studies to determine the role of reactive oxygen species versus the presence of Cu and/or Zn in the effects observed here could involve performing pretreatment with anti-oxidants, additional Cu and Zn controls, measuring calcium flux and channel expression, and further experiments using BMP6 antagonists (e.g., Noggin) or iron. In addition, testing whether inhibition of active microtubule formation (e.g., via Cytochalasin B) may abrogate motility, would certainly help clarify whether the enhanced motility is due to electric field, as it has been shown for electric-field-mediated motility [32]. Furthermore, it would be interesting to test if application of the microparticles enhances cell migration in response to chemokines (as opposed to electric field), and in particular to physiological wound-healing cytokines such as platelet-derived growth factor, which has been shown to induce fibroblast transmigration in previous studies [87].

Furthermore, given that results of this study might also have implications to the use of topical low-grade electric fields via microparticles for wound healing, interesting areas of future work could also include optimization of the electric and chemical enhancement of cell migration, as well as further examining possible effects of the galvanic microparticles on cell proliferation. In this study, scratches were performed through the middle of confluent wells of fibroblasts, which exhibited a characteristic swirling pattern, and so the wounds

were therefore in random directions with respect to the swirl as it passed through our region of interest. Given the known role of cell polarity in wound healing, it would be interesting, in future studies, to perform systematic studies of wounds made on confluent layers of fibroblasts and/or endothelial cells with controlled orientation and for longer time points so that the effects of the galvanic microparticles on cell division and polarity may be studied.

Finally, investigating the potential use of galvanic microparticles in model systems involving other tissue types known to be responsive to electrical stimulation (e.g., bone, neural etc.) with or without patterning the distribution of microparticles, as well as expanding *in vivo* studies will be key towards applying these results in a broader regenerative medicine context.

Acknowledgments

We gratefully acknowledge Grace Chao for providing advice with wound healing experiments, Christian Landeros, Kevin Tulod and Surapon Charoensook for help with initial studies. The work was funded in part by NIH grant EB002520.

References

1. Plonsey, R.; Barr, RC. Bioelectricity: A Quantitative Approach. Springer Science; New York: 2007.
2. Levin M, Stevenson CG. Regulation of cell behavior and tissue patterning by bioelectrical signals: challenges and opportunities for biomedical engineering. Annual Review of Biomedical Engineering. 2012; 14:295–323.
3. Du Bois-Reymond E. Vorläufiger Abriss einer Untersuchung uber den sogenannten Froschstrom und die electomotorischen Fische. Annales Physique und Chemie. 1843; 58:1–30.
4. Slack JMW. The spark of life: electricity and regeneration. Science Signal Transduction Knowledge Environment. 2007; 2007:pe54.
5. McCaig CD, Rajnicek AM, Song B, Zhao M. Controlling cell behavior electrically: current views and future potential. Physiological Reviews. 2005; 85:943–978. [PubMed: 15987799]
6. Nuccitelli R. Physiological electric fields can influence cell motility, growth, and polarity. Advances in Molecular and Cell Biology. 1988; 2:213–233.
7. Robinson KR. The responses of cells to electrical fields: a review. Journal of Cell Biology. 1985; 101:2023–2027. [PubMed: 3905820]
8. Sugimoto M, Maeshige N, Honda H, Yoshikawa Y, Uemura M, Yamamoto M, et al. Optimum microcurrent stimulation intensity for galvanotaxis in human fibroblasts. Journal of Wound Care. 2012; 21:5–6. [PubMed: 22240927]
9. Guo A, Song B, Reid B, Gu Y, Forrester JV, Jahoda CA, et al. Effects of physiological electric fields on migration of human dermal fibroblasts. Journal of Investigative Dermatology. 2010; 130:2320–2327. [PubMed: 20410911]
10. Song S, Han H, Ko UH, Kim J, Shin JH. Collaborative effects of electric field and fluid shear stress on fibroblast migration. Lab on a Chip. 2013; 13:1602–1611. [PubMed: 23450300]
11. Nishimura KY, Isseroff RR, Nuccitelli R. Human keratinocytes migrate to the negative pole in direct current electric fields comparable to those measured in mammalian wounds. Journal of Cell Science. 1996; 109:199–207. [PubMed: 8834804]
12. Fang KS, Farboud B, Nuccitelli R, Isseroff RR. Migration of human keratinocytes in electric fields requires growth factors and extracellular calcium. Journal of Investigative Dermatology. 1998; 111:751–756. [PubMed: 9804333]
13. Grahn JC, Reilly DA, Nuccitelli RL, Isseroff RR. Melanocytes do not migrate directionally in physiological DC electric fields. Wound Repair and Regeneration. 2003; 11:64–70. [PubMed: 12581428]

14. Zhao M. Electrical fields in wound healing—An overriding signal that directs cell migration. Seminars in Cell & Developmental Biology. 2009; 20:674–682. [PubMed: 19146969]
15. Messerli MA, Graham DM. Extracellular electrical fields direct wound healing and regeneration. Biological Bulletin. 2011; 221:79–92. [PubMed: 21876112]
16. Karba R, Šemrov D, Vodovnik L, Benko H, Šavrin R. DC electrical stimulation for chronic wound healing enhancement Part 1. Clinical study and determination of electrical field distribution in the numerical wound model. Bioelectrochemistry and Bioenergetics. 1997; 43:265–270.
17. Kaur S, Lyte P, Garay M, Liebel F, Sun Y, Liu JC, et al. Galvanic zinc-copper microparticles produce electrical stimulation that reduces the inflammatory and immune responses in skin. Archiv fur Dermatologische Forschung (Archives for Dermatological Research). 2011; 303:551–562.
18. Werner S, Krieg T, Smola H. Keratinocyte–fibroblast interactions in wound healing. Journal of Investigative Dermatology. 2007; 127:998–1008. [PubMed: 17435785]
19. Werner S, Krieg T, Smola H. Keratinocyte–fibroblast interactions in wound healing. Journal of Investigative Dermatology. 2006; 127:998–1008. [PubMed: 17435785]
20. Voldman J. Electrical forces for microscale cell manipulation. Annual Review of Biomedical Engineering. 2006; 8:425–454.
21. Bronzino, JD. The Biomedical Engineering Handbook. 1995.
22. Cannizzaro, C.; Tandon, N.; Figallo, E.; Park, H.; Gerecht, S.; Radisic, M.; Elvassore, N.; Vunjak-Novakovic, G. Practical aspects of cardiac tissue engineering with electrical stimulation. In: Hauser, H.; Fussenegger, M., editors. Methods in Molecular Medicine, Tissue Engineering. Humana Press; Totowa, NJ: 2007. p. 291-307.
23. Tandon N, Cannizzaro C, Chao PHG, Maidhof R, Marsano A, Au HTH, et al. Electrical stimulation systems for cardiac tissue engineering. Nature Protocols. 2009; 4:155–173.
24. Eruslanov E, Kusmartsev S. Identification of ROS using oxidized DCFDA and flow-cytometry. Methods in Molecular Biology. 2010; 594:57–72. [PubMed: 20072909]
25. Chao PH, Lu HH, Hung CT, Nicoll SB, Bulinski JC. Effects of applied DC electric field on ligament fibroblast migration and wound healing. Connective Tissue Research. 2007; 48:188–197. [PubMed: 17653975]
26. Atkins, P.; dePaula, J. Atkins' Physical Chemistry. 8. Oxford University Press; 2006. Working Galvanic cells.
27. Ahmad, Z. Principles of Corrosion Engineering and Corrosion Control (Google Book). 2006.
28. Merrill DR, Bikson M, Jefferys JG. Electrical stimulation of excitable tissue: design of efficacious and safe protocols. Journal of Neuroscience Methods. 2005; 141:171–198. [PubMed: 15661300]
29. Ligier V, Wéry M, Hihn JY, Faucheu J, Tachez M. Formation of the main atmospheric zinc end products: $NaZn_4Cl$ (OH) $6SO_4 \cdot 6H_2O$, Zn_4SO_4 $(OH)_6 \cdot nH_2O$ and Zn_4Cl_2 (OH) $4SO_4 \cdot 5H_2O$ in [Cl-][$SO_2{}^{-4}$][HCO^{-3}][H_2O_2] electrolytes. Corrosion Science. 1999; 41:1139–1164.
30. Zhao M, Song B, Pu J, Wada T, Reid B, Tai G, et al. Electrical signals control wound healing through phosphatidylinositol-3-OH kinase-gamma and PTEN. Nature. 2006; 442:457–460. [PubMed: 16871217]
31. Eckes B, Zweers MC, Zhang ZG, Hallinger R, Mauch C, Aumailley M, et al. Mechanical tension and integrin α2β1 regulate fibroblast functions. Journal of Investigative Dermatology Symposium Proceedings. 2006; 11:66–72.
32. Finkelstein E, Chang W, Chao PHG, Gruber D, Minden A, Hung CT, et al. Roles of microtubules, cell polarity and adhesion in electric-field-mediated motility of 3T3 fibroblasts. Journal of Cell Science. 2004; 117:1533–1545. [PubMed: 15020680]
33. Kucerova R, Walczysko P, Reid B, Ou J, Leiper LJ, Rajnicek AM, et al. The role of electrical signals in murine corneal wound re-epithelialization. Journal of Cellular Physiology. 2011; 226:1544–1553. [PubMed: 20945376]
34. Song B, Zhao M, Forrester JV, McCaig CD. Electrical cues regulate the orientation and frequency of cell division and the rate of wound healing in vivo. Proceedings of the National Academy of Sciences. 2002; 99:13577–13582.
35. Sussman, CDP.; Bates-Jensen, BP. Wound Care: A Collaborative Practice Manual for Health Professionals. 3. 2006. Chapter 2: Wound healing physiology: acute and chronic.

36. Serena E, Figallo E, Tandon N, Cannizzaro C, Gerecht S, Elvassore N, et al. Electrical stimulation of human embryonic stem cells: cardiac differentiation and the generation of reactive oxygen species. Experimental Cell Research. 2009; 315:3611–3619. [PubMed: 19720058]
37. Sauer H, Rahimi G, Hescheler J, Wartenberg M. Effects of electrical fields on cardiomyocyte differentiation of embryonic stem cells. Journal of Cellular Biochemistry. 1999; 75:710–723. [PubMed: 10572253]
38. Hronik-Tupaj M, Rice W, Cronin-Golomb M, Kaplan D, Georgakoudi I. Osteoblastic differentiation and stress response of human mesenchymal stem cells exposed to alternating current electric fields. Biomedical Engineering Online. 2011; 10:9. [PubMed: 21269490]
39. Sen CK, Roy S. Redox signals in wound healing. Biochimica et Biophysica Acta (BBA)—General Subjects. 2008; 1780:1348–1361.
40. Hurd TR, DeGennaro M, Lehmann R. Redox regulation of cell migration and adhesion. Trends in Cell Biology. 2012; 22:107–115. [PubMed: 22209517]
41. Setsukinai KI, Urano Y, Kakinuma K, Majima HJ, Nagano T. Development of novel fluorescence probes that can reliably detect reactive oxygen species and distinguish specific species. Journal of Biological Chemistry. 2003; 278:3170–3175. [PubMed: 12419811]
42. Kaur S, Lyte P, Garay M, Liebel F, Sun Y, Liu JC, et al. Galvanic zinc–copper microparticles produce electrical stimulation that reduces the inflammatory and immune responses in skin. Archives of Dermatological Research. 2011; 303:551–562. [PubMed: 21465312]
43. Haliwell, B.; Gutteridge, J. Free Radicals in Biology and Medicine. Oxford University Press; Oxford, UK: 2005.
44. Chevion M, Korbashi P, Katzhandler J, Saltman P. Zinc—a redox-inactive metal provides a novel approach for protection against metal-mediated free radical induced injury: study of paraquat toxicity in *E. coli*. Advances in Experimental Medicine and Biology. 1990; 264:217–222. [PubMed: 2244499]
45. Aust, AE.; Eveleigh, JF. Proceedings of the Society for Experimental Biology and Medicine. Society for Experimental Biology and Medicine; New York, NY: 1999. Mechanisms of DNA oxidation; p. 246-252.
46. Sies H. Oxidative stress: oxidants and antioxidants. Experimental Physiology. 1997; 82:291–295. [PubMed: 9129943]
47. Murrell GA, Francis M, Bromley L. Modulation of fibroblast proliferation by oxygen free radicals. Biochemical Journal. 1990; 265:659. [PubMed: 2154966]
48. Niethammer P, Grabher C, Look AT, Mitchison TJ. A tissue-scale gradient of hydrogen peroxide mediates rapid wound detection in zebrafish. Nature. 2009; 459:996–999. [PubMed: 19494811]
49. Cook-Mills JM, Marchese ME, Abdala-Valencia H. Vascular cell adhesion molecule-1 expression and signaling during disease: regulation by reactive oxygen species and antioxidants. Antioxidants and Redox Signaling. 2011; 15:1607–1638. [PubMed: 21050132]
50. Frey RS, Ushio-Fukai M, Malik AB. NADPH oxidase-dependent signaling in endothelial cells: role in physiology and pathophysiology. Antioxidants and Redox Signaling. 2009; 11:791–810. [PubMed: 18783313]
51. Oshikawa J, Urao N, Kim HW, Kaplan N, Razvi M, McKinney R, et al. Extracellular SOD-derived H_2O_2 promotes VEGF signaling in caveolae/lipid rafts and post-ischemic angiogenesis in mice. PLoS One. 2010; 5:e10189. [PubMed: 20422004]
52. Goldkorn T, Balaban N, Matsukuma K, Chea V, Gould R, Last J, et al. EGF-receptor phosphorylation and signaling are targeted by H_2O_2 redox stress. American Journal of Respiratory Cell and Molecular Biology. 1998; 19:786. [PubMed: 9806743]
53. van der Vliet A, Hristova M, Cross CE, Eiserich JP, Goldkorn T. Peroxynitrite induces covalent dimerization of epidermal growth factor receptors in A431 epidermoid carcinoma cells. Journal of Biological Chemistry. 1998; 273:31860–31866. [PubMed: 9822654]
54. Lambert S, Ameels H, Gniadecki R, Hérin M, Poumay Y. Internalization of EGF receptor following lipid rafts disruption in keratinocytes is delayed and dependent on p38 MAPK activation. Journal of Cellular Physiology. 2008; 217:834–845. [PubMed: 18727093]
55. Lukyanov, KA.; Belousov, VV. Genetically encoded fluorescent redox sensors. Biochimica et Biophysica Acta. http://dx.doi.org/10.1016/j.bbagen.2013.05.030, in press

56. Yoo SK, Freisinger CM, LeBert DC, Huttenlocher A. Early redox, Src family kinase, and calcium signaling integrate wound responses and tissue regeneration in zebrafish. Journal of Cell Biology. 2012; 199:225–234. [PubMed: 23045550]
57. Midwood KS, Williams LV, Schwarzbauer JE. Tissue repair and the dynamics of the extracellular matrix. International Journal of Biochemistry & Cell Biology. 2004; 36:1031–1037. [PubMed: 15094118]
58. Porter S. The role of the fibroblast in wound contraction and healing. Wounds UK. 2007; 3:33.
59. Werner S, Grose R. Regulation of wound healing by growth factors and cytokines. Physiological Reviews. 2003; 83:835–870. [PubMed: 12843410]
60. Kamata H, Oka S, Shibukawa Y, Kakuta J, Hirata H. Redox regulation of nerve growth factor-induced neuronal differentiation of PC12 cells through modulation of the nerve growth factor receptor. TrkA, Archives of Biochemistry and Biophysics. 2005; 434:16–25.
61. Corradini E, Meynard D, Wu Q, Chen S, Ventura P, Pietrangelo A, et al. Serum and liver iron differently regulate the bone morphogenetic protein 6 (BMP6)-SMAD signaling pathway in mice. Hepatology. 2011; 54:273–284. [PubMed: 21488083]
62. Cornelissen, L. Which molecules of the initial phase of wound healing may be used as markers for early detection of skin damage. Materials Technology Institute: Eindhoven University of Technology; Eindhoven, Netherlands: 2004.
63. Kaiser S, Schirmacher P, Philipp A, Protschka M, Moll I, Nicol K, et al. Induction of bone morphogenetic protein-6 in skin wounds. Delayed reepitheliazation and scar formation in BMP-6 overexpressing transgenic mice. Journal of Investigative Dermatology. 1998; 111:1145–1152. [PubMed: 9856831]
64. Miyazono K, Kamiya Y, Morikawa M. Bone morphogenetic protein receptors and signal transduction. Journal of Biochemistry. 2010; 147:35–51. [PubMed: 19762341]
65. Wagner DO, Sieber C, Bhushan R, Borgermann JH, Graf D, Knaus P. BMPs: from bone to body morphogenetic proteins. Science Signaling. 2010; 3:mr1. [PubMed: 20124549]
66. Botchkarev VA. Bone morphogenetic proteins and their antagonists in skin and hair follicle biology[ast]. Journal of Investigative Dermatology. 2003; 120:36–47. [PubMed: 12535196]
67. Hirt-Burri N, Scaletta C, Gerber S, Pioletti DP, Applegate LA. Wound-healing gene family expression differences between fetal and foreskin cells used for bioengineered skin substitutes. Artificial Organs. 2008; 32:509–518. [PubMed: 18638304]
68. Kaiser S, Schirmacher P, Philipp A, Protschka M, Moll I, Nicol K, et al. Induction of bone morphogenetic protein-6 in skin wounds. Delayed reepitheliazation and scar formation in BMP-6 overexpressing transgenic mice. Journal of Investigative Dermatology. 1998; 111:1145–1152. [PubMed: 9856831]
69. Chen D, Zhao M, Mundy GR. Bone morphogenetic proteins. Growth Factors. 2004; 22:233–241. [PubMed: 15621726]
70. Owens P, Han G, Li AG, Wang XJ. The role of Smads in skin development. Journal of Investigative Dermatology. 2008; 128:783–790. [PubMed: 18337711]
71. Han G, Li F, ten Dijke P, Wang X-J. Temporal Smad7 transgene induction in mouse epidermis accelerates skin wound healing. American Journal of Pathology. 2011; 179:1768–1779. [PubMed: 21944279]
72. Valdimarsdottir G, Goumans MJ, Rosendahl A, Brugman M, Itoh S, Lebrin F, et al. Stimulation of Id1 expression by bone morphogenetic protein is sufficient and necessary for bone morphogenetic protein-induced activation of endothelial cells. Circulation. 2002; 106:2263–2270. [PubMed: 12390958]
73. Rotzer D, Krampert M, Sulyok S, Braun S, Stark HJ, Boukamp P, et al. Id proteins: novel targets of activin action, which regulate epidermal homeostasis. Oncogene. 2006; 25:2070–2081. [PubMed: 16288215]
74. Pache G, Schafer C, Wiesemann S, Springer E, Liebau M, Reinhardt HC, et al. Upregulation of Id-1 via BMP-2 receptors induces reactive oxygen species in podocytes. American Journal of Physiology—Renal Physiology. 2006; 291:F654–F662. [PubMed: 16622178]
75. Camaschella C. BMP6 orchestrates iron metabolism. Nature Genetics. 2009 Apr.41:386–388. [PubMed: 19338078]

76. Kautz L, Meynard D, Monnier A, Darnaud V, Bouvet R, Wang RH, et al. Iron regulates phosphorylation of Smad1/5/8 and gene expression of Bmp6, Smad7, Id1, and Atoh8 in the mouse liver. Blood. 2008; 112:1503–1509. [PubMed: 18539898]

77. Bissett DL, McBride JF. Iron content of human epidermis from sun-exposed and non-exposed body sites. Journal—Society Of Cosmetic Chemists. 1992; 43:215.

78. Bissett DL, McBride JF. Synergistic topical photoprotection by a combination of the iron chelator 2-furildioxime and sunscreen. Journal of the American Academy of Dermatology. 1996; 35:546–549. [PubMed: 8859281]

79. Polefka T, Bianchini R, Shapiro S. Interaction of mineral salts with the skin: a literature survey. International Journal of Cosmetic Science. 2012; 34:416–423. [PubMed: 22712689]

80. Keen CL, Uriu-Hare JY, Hawk SN, Jankowski MA, Daston GP, Kwik-Uribe CL, et al. Effect of copper deficiency on prenatal development and pregnancy outcome. American Journal of Clinical Nutrition. 1998; 67:1003S–1011S. [PubMed: 9587143]

81. Black RE. Micronutrients in pregnancy. British Journal of Nutrition. 2001; 85:S193–S197. [PubMed: 11509110]

82. Tenaud I, Sainte-Marie I, Jumbou O, Litoux P, Dreno B. In vitro modulation of keratinocyte wound healing integrins by zinc, copper and manganese. British Journal of Dermatology. 1999; 140:26–34. [PubMed: 10215764]

83. Mirastschijski U, Martin A, Jorgensen LN, Sampson B, Agren MS. Zinc, copper, and selenium tissue levels and their relation to subcutaneous abscess, minor surgery, and wound healing in humans. Biological Trace Element Research. 2013; 153:76–83. [PubMed: 23595590]

84. Myers S, Nield A, Myers M. Zinc transporters, mechanisms of action and therapeutic utility: implications for type 2 diabetes mellitus. Journal of Nutrition and Metabolism. 2012; 2012:Article ID: 173712, 13.

85. Wee NK, Weinstein DC, Fraser ST, Assinder SJ. The mammalian copper transporters CTR1 and CTR2 and their roles in development and disease. International Journal of Biochemistry & Cell Biology. 2013; 45:960–963. [PubMed: 23391749]

86. Mor M, Beharier O, Levy S, Kahn J, Dror S, Blumenthal D, Gheber LA, Peretz A, Katz A, Moran A, Etzion Y. ZnT-1 enhances the activity and surface expression of T-type calcium channels through activation of Ras-ERK signaling. American Journal of Physiology—Cell Physiology. 2012; 303:C192–C203. [PubMed: 22572848]

87. Greiling D, Clark R. Fibronectin provides a conduit for fibroblast transmigration from collagenous stroma into fibrin clot provisional matrix. Journal of Cell Science. 1997; 110:861–870. [PubMed: 9133673]

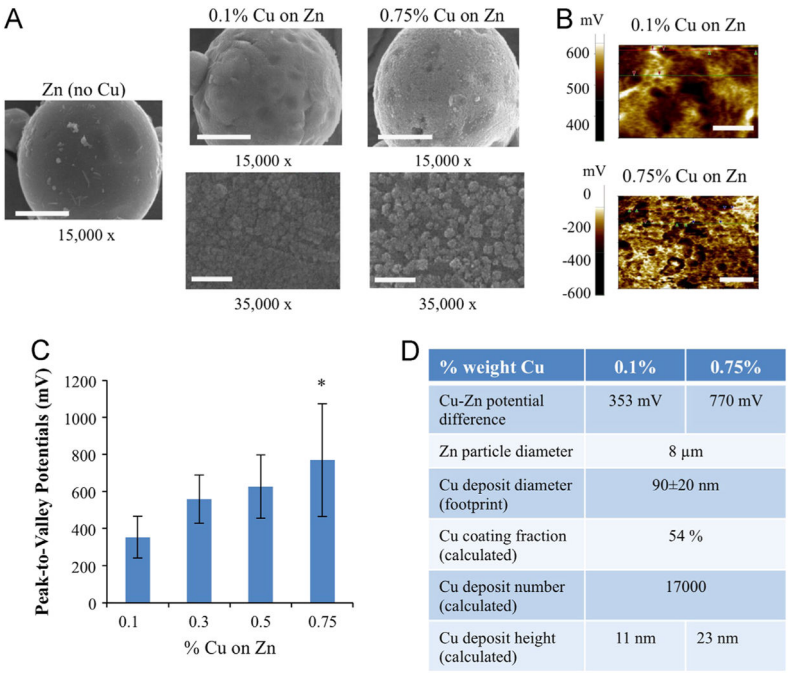

% weight Cu	0.1%	0.75%
Cu-Zn potential difference	353 mV	770 mV
Zn particle diameter	8 μm	
Cu deposit diameter (footprint)	90±20 nm	
Cu coating fraction (calculated)	54 %	
Cu deposit number (calculated)	17000	
Cu deposit height (calculated)	11 nm	23 nm

Fig. 1.

Characterization and modeling of galvanic microparticles. (A) Scanning electron microscope (SEM) micrographs of galvanic microparticles of Zn, 0.1% Cu on Zn, and 0.75% Cu on Zn, at 15,000 × and 35,000 × magnification, respectively. Scale bars for micrographs at 15,000 × and 35,000 × magnification correspond to 3 μm, and 1 μm, respectively. (B) Scanning Kelvin probe microscopy (SKPM) images of Zn surface coated by copper specks amounting to 0.1% and 0.75% weight Cu, respectively. Scale bars correspond to 500 nm and 1 μm, respectively. (C) Peak-to-valley potentials calculated via surface potential analysis of SKPM images for a range of Cu coatings (0.1%–0.75% of Cu on Zn). *denotes *p*-value <0.001 (*T*-test). (D) Parameters determined from SEM and SKPM data for 0.1% and 0.75% Cu on Zn, respectively.

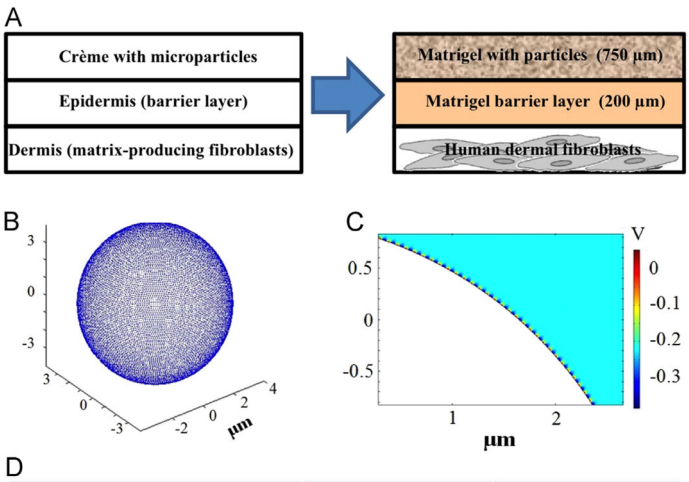

D

% weight Cu	0.1%	0.75%
Particle Radius (µm)	4.0	
Particle Volume (µm³)	268	
Particle Density (g/cm³)	7.14	
Particle Weight (ng)	1.91	
# Particles/mg	5.22×10^5	
Galvanic Current (µA/mg)	80[1]	175[2]
Galvanic Current / particle (pA)	153	335
Current in single well of 24-well plate		
Concentration (weight/volume)		
0.05% (µA)	6.0	13.1
0.005% (µA)	0.6	1.31
0.0005% (nA)	60	131

[1] Kaur, et al. Arch Dermatol Res. 2011 Oct;303(8):551-62.
[2] Calculated in proportion to measured peak-to-valley potentials from **Fig 1**

Fig. 2.

Model system. (A) Human dermal fibroblasts were subjected to Zn–Cu galvanic microparticles, in a three-layer system designed to mimic the application of crème containing microparticles to human skin. (B) Three-Dimensional model of semispherical Cu specks (radius = 0.5 µm) on a Zn particle (diameter = 8 µm). (C) Two-Dimensional finite-element model color map of electric potential surrounding a 0.75% Cu on Zn particle. (D) Calculated currents and intermediate parameters for varying concentrations of microparticles within the model system.

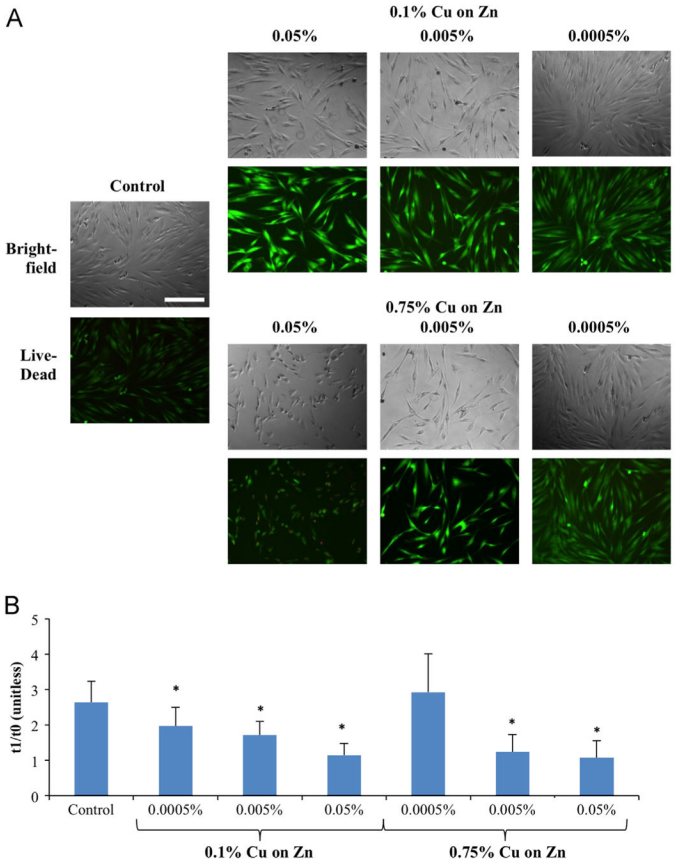

Fig. 3.

Cellular viability and survival of human dermal fibroblasts cultured with galvanic microparticles. Data are shown at 24 h of cultivation, with the pre-culture data used as a control. (A) Bright field (top) and live/dead fluorescence images (bottom) (scale bar corresponds to 500 μm). (B) Plot of cells counted after 24 h culture with galvanic microparticles, as compared with control samples at t0. Data shown are mean±standard deviation from 3 independent experiments with $n = 5$ each (*$p \leq 0.05$ compared to control at 24 h).

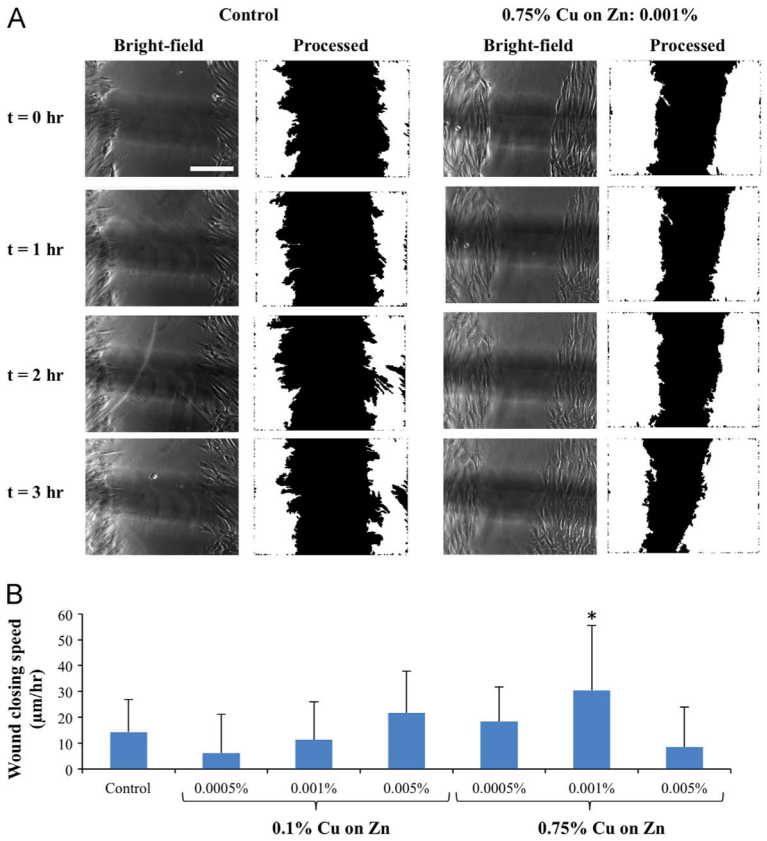

Fig. 4.

fiWound healing assay. (A) Phase contrast images (left) and the corresponding processed images (right) used for determining the speed of closing of the wound edges at t = 0, 1, 2, and 3 h after the application of Zn–Cu galvanic microparticles (scale bar corresponds to 500 μm). (B) Wound closure speed computed from the phase contrast images for varying concentrations of applied Zn–Cu galvanic microparticles. Data from three independent experiments with n = 13–24 per group were pooled for the determination of each data point (*p<0.05 compared to control).

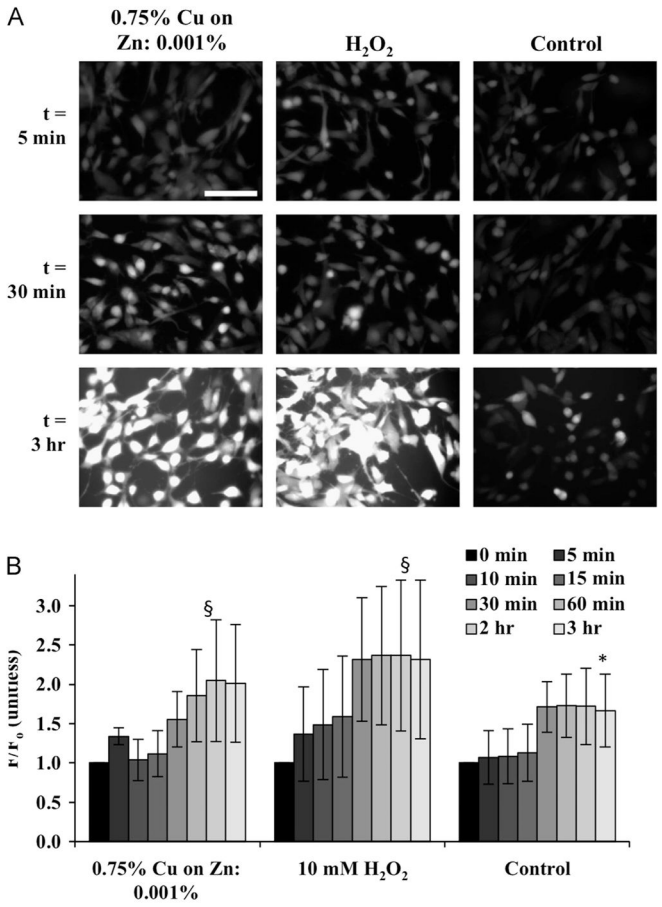

Fig. 5.

Effect of galvanic microparticles generation of reactive oxygen species (ROS). Data for the corresponding cell cultures subjected to H_2O_2 and unstimulated controls are shown for comparison. (A) Fluorescence images of human dermal fibroblasts loaded with dichlorofluorescein (DCF) after application of microparticles or H_2O_2 (scale bar: 500 μm). (B) The time course of ROS generation (measured from DCF intensity) that was normalized by the intensity at time 0. For each time point, data were obtained from three independent experiments with $n = 3$ samples each and 9 measurements for each sample. $^{*}p<0.05$ between timepoint and $t = 5$ min; $^{\S}p<0.05$ both between time point and $t = 5$ min, and between same time points for the control and experimental condition.

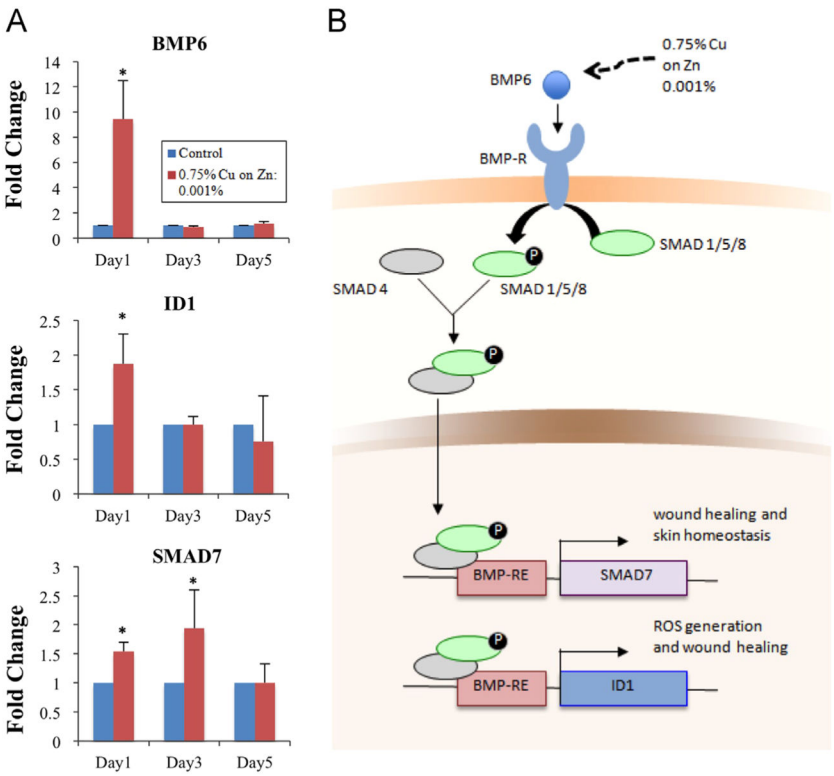

Fig. 6.

Gene expression profiles. (A) RNA levels for BMP6, ID1 and SMAD7 shown relatively to the housekeeper gene (GAPDH) (*$p \leq 0.05$ compared to control). (B) The proposed role of BMP6 signaling pathway, acting via ID1 and SMAD7 in stimulating ROS, wound healing, and homeostasis.